VIP Thermoresponsive Materials Very Important Paper

How to cite: *Angew. Chem. Int. Ed.* **2020**, *59*, 12455–12459
International Edition: doi.org/10.1002/anie.202003991
German Edition: doi.org/10.1002/ange.202003991

Interlocked DNA Nanojoints for Reversible Thermal Sensing

*Yinzhou Ma[+], Mathias Centola[+], Daniel Keppner, and Michael Famulok**

In memory of Professor Rolf Huisgen

Abstract: *The ability to precisely measure and monitor temperature at high resolution at the nanoscale is an important task for better understanding the thermodynamic properties of functional entities at the nanoscale in complex systems, or at the level of a single cell. However, the development of high-resolution and robust thermal nanosensors is challenging. The design, assembly, and characterization of a group of thermal-responsive deoxyribonucleic acid (DNA) joints, consisting of two interlocked double-stranded DNA (dsDNA) rings, is described. The DNA nanojoints reversibly switch between the static and mobile state at different temperatures without a special annealing process. The temperature response range of the DNA nanojoint can be easily tuned by changing the length or the sequence of the hybridized region in its structure, and because of its interlocked structure the temperature response range of the DNA nanojoint is largely unaffected by its own concentration; this contrasts with systems that consist of separated components.*

Deoxyribonucleic acid (DNA) has been applied as a versatile building material for constructing various nanoarchitectures in a bottom-up approach because of its unique self-recognition and its suitability to be chemically modified. The flexibility and programmability provided by DNA allows dynamic functional architectures to be established that can respond to different stimuli, such as pH,[1] oligo-(deoxy)nucleotides (ODNs),[2] light,[3] and temperature.[4] Among them, thermoresponsive systems that fully depend on the thermodynamic stability of DNA have been reported in living organisms,[5] illustrating their high potential for biomedical applications. In recent years, thermoresponsive DNA architectures have been widely used as sensors,[2–4] DNA nanothermometers,[4c] for cargo-delivery,[4b,d,f] and as temperature-sensitive hydrogel.[4e] However, the thermo-responsive mechanism of DNA architectures relies on the breakage of hydrogen bonds between nucleobases and the unwinding of double-stranded DNA (dsDNA) at specific temperatures, which often leads to their partial or complete disassembly[4a,c,e,f] and requires special annealing methods to reverse the process and yield the original nanosystems.[4c,e]

DNA catenanes are stable mechanically interlocked structures that provide an ideal platform for overcoming these limitations. In recent years, DNA catenanes have been widely used as switchable joints,[6] reversible logic circuits,[1c] and molecular motors[7] because of their mobility. Unlike static DNA architectures, DNA catenanes consist of two or more individual DNA rings that are connected through mechanical bonds that permit high rotational degrees of freedom and allow them to move independently relative to each other.[7a,8] Previous studies showed that DNA catenanes can be reversibly switched between a static hybridized (Cat^{hyb}) state and a mobile non-hybridized mechanically interlocked (Cat^{mec}) state through different stimuli, such as ions[6a] and pH changes,[6a] or by means of strand displacement.[1b,8] However, thermal stimuli have not yet been used for controlling the conversion from a Cat^{hyb} to a Cat^{mec} by selectively melting only the hybridizing portion between the rings constituting the hybridized and mechanically interlocked nanostructure, instead of dehybridizing the complete catenane structure. Herein, we present the design, synthesis, and characterization of a group of DNA nanostructures with thermal-responsive junctions. The described thermal-responsive DNA [2]catenanes consist of two interlocked dsDNA rings that are hybridized with each other through a pair of single-stranded regions (ss-regions) on each DNA ring and can reversibly interchange between the static and the mobile state at different temperatures.

The assembly of the catenanes is illustrated in Figure 1 a. In the first step, a dsDNA ring (ring A) with two ss-regions (a1 and a2) is assembled from ODNs by thermal annealing. To achieve the mechanically interlocked structure, an ODN from the second dsDNA ring (ring B) is threaded through ring A and hybridizes to it through the complementary ss-region a1 and b1. The remaining ODNs of ring B are added to form the second dsDNA ring (ring B) also containing two ss-regions (b1 and b2), resulting in a Cat^{hyb}. To enhance the stability of the whole structure, all ODNs are enzymatically ligated using T4 DNA ligase. The rings are designed[9] to increase the threading of the ODN through ring A; nevertheless, some will hybridize without threading through the ring and will result in

[*] Dr. Y. Ma,[+] M. Centola,[+] D. Keppner, Prof. Dr. M. Famulok
LIMES Chemical Biology Unit, Universität Bonn
Gerhard-Domagk-Straße 1, 53121 Bonn (Germany)
E-mail: m.famulok@uni-bonn.de
M. Centola,[+] Prof. Dr. M. Famulok
Center of Advanced European Studies and Research
Ludwig-Erhard-Allee 2, 53175 Bonn (Germany)
[+] These authors contributed equally to this work.

Supporting information, including experimental details and the ORCID identification number(s) for the author(s) of this article, can be found under:
https://doi.org/10.1002/anie.202003991.

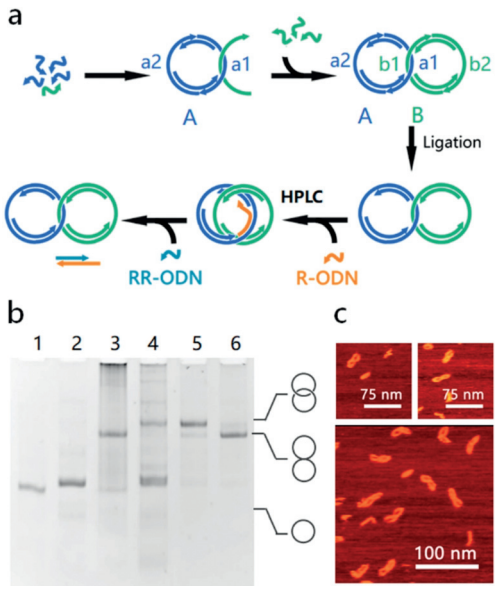

Figure 1. Assembly and characterization of the Cat^{hyb}. a) Schematic for a Cat^{hyb} assembly. b) Analysis of Cat^{hyb} assembly with 6% native PAGE. Lane 1, ring A; lane 2, ring B; lane 3, catenane after ligation; lane 4, catenane after addition of R-ODN; lane 5, catenane purified by weak anion exchange HPLC; lane 6, catenane after adding RR-ODN. c) AFM images of the hybridized [2]catenane.

hybridized but not mechanically interlocked [2]catenanes. To separate these from the properly assembled catenanes, a so-called "release ODN" (R-ODN) is added, which has a complementary sequence to the ss-region a1 of ring A and can separate ring B from ring A through toehold-mediated strand displacement. Consequently, the Cat^{hyb} is converted into a Cat^{mec}. Only in mechanically interlocked catenanes, the two rings will stay interlocked while all the non-interlocked two-ring hybrids will disassemble into the two rings. The Cat^{mec} can be separated from dsDNA rings by weak anion-exchange high-performance liquid chromatography (HPLC) purification (Supporting Information, Table S1). After purification, a so-called "reverse ODN" (RR-ODN), which is complementary to R-ODN, is added to remove R-ODN from the ss-region a1, allowing ring B to hybridize again to ring A and restore the Cat^{hyb} (for sequences see the Supporting Information, Figure S1, Tables S2 and S3).

The assembly process and switching between the Cat^{hyb} and Cat^{mec} was characterized by 6% native polyacrylamide gel electrophoresis (PAGE; Figure 1b). After the R-ODN was added (Figure 1b, lane 4), the migration of the [2]catenane became slower, indicating the Cat^{hyb} to Cat^{mec} conversion.[8a,10] Furthermore, the band of DNA rings became more intense, suggesting that the hybridized but non-interlocked DNA rings have been separated into the two individual DNA rings by the addition of the R-ODN. After RR-ODN was added to the HPLC-purified product (Figure 1b, lane 6), the electrophoretic mobility of the [2]catenane was restored to that of the [2]catenane prior to the addition of R-ODN (Figure 1b, lane 3) indicating that the Cat^{mec} had been converted into the Cat^{hyb}. Tapping mode atomic force microscopy (AFM) analysis in liquid also confirmed the formation of the hybridized catenane (Figure 1c; Figure S2).

The thermal switching behavior of the Cat^{hyb} is controlled by the melting temperature (T_m) of the hybridized region (HR) between ss-regions a1 and b1. T_m can be defined as the temperature at which half of the HR is dissociated to single-stranded DNA (ssDNA), and in this case generates the Cat^{mec}. To examine the switching process of the Cat^{hyb}, we labeled two ODNs from the DNA architecture with the fluorophore (6-FAM) on one ring and the quencher (BHQ®-1) on the other ring (Figure 2a). Below the T_m, the HR largely remains in the hybridized state with the fluorophore and quencher in close proximity, leading to a low fluorescence intensity. As temperature increases HR begins to melt and the Cat^{hyb} is converted into the Cat^{mec}. In that state, fluorophore and quencher separate, an increase of fluorescence intensity results. As a proof of concept, we first designed a Cat^{hyb} with a nine base pairs hybridization sequence in its HR (named G9, the sequence is shown in Table 1).

Table 1: Sequences of different HRs in the Cat^{hyb}.

HR domains	Sequence	Length [nt]	GC content	T_m [°C]
G5T5	a1: 5′-AAAAAGCGCC-3′ b1: 3′-TTTTTCGCGG-5′	10	50.0%	37.00 ± 0.04
G7T2	a1: 5′-CGCAGAGCC-3′ b1: 3′-GCGTCTCGG-5′	9	77.8%	40.50 ± 0.02
G7T3	a1: 5′-CCTGCTGCTC-3′ b1: 3′-GGACGACGAG-5′	10	70.0%	47.50 ± 0.02
G9	a1: 5′-CGCCGGGCC-3′ b1: 3′-GCGGCCCGG-3′	9	100.0%	55.00 ± 0.02

As shown in Figure 2b (red curve), in the DNA catenane buffer (DC buffer: 10 mM Tris-HCl, 1 mM ethylenediaminetetraacetic acid (EDTA), 25 mM $MgCl_2$, pH 8.0) the fluorescence intensity of the Cat^{hyb}-G9 increased as the temperature rose from 42 °C to 62 °C, indicating the melting of the HR and conversion of the static Cat^{hyb}-G9 to the mobile Cat^{mec}. The red curve indicates that the Cat^{hyb}-G9 is fully converted into Cat^{mec} at 62 °C. However, above 62 °C the fluorescence intensity of the Cat^{hyb}-G9 began to decrease with further rising temperature, which is consistent with a phenomenon that was previously observed to be a temperature-dependent characteristic of 6-FAM.[11] Similarly, we observed an influence of temperature on the emitted non-quenched fluorescence signal also with a different fluorophore (Figure S4) or in a different buffer system (Figure S5). As expected, the fluorescence intensity of a Cat^{mec} positive control that has a non-quenched 6-FAM, also decreased with increasing temperature (Figure 2b, black curve). This curve allows distinguishing the temperature-dependent fluorescence of FAM alone from the overall fluorescence changes that are caused by the conversion from Cat^{hyb} into the mechanically interlocked DNA nanojoint. The fluorescence intensity of the "Y"-shaped negative control (Figure 2b, blue curve) containing a 24 bp HR (Figure 2c; Figure S3), remained unchanged when the temperature rose from 42 °C to 62 °C, indicating constant FAM quenching because of the stable fluorophore and quencher arrangement in this structure.

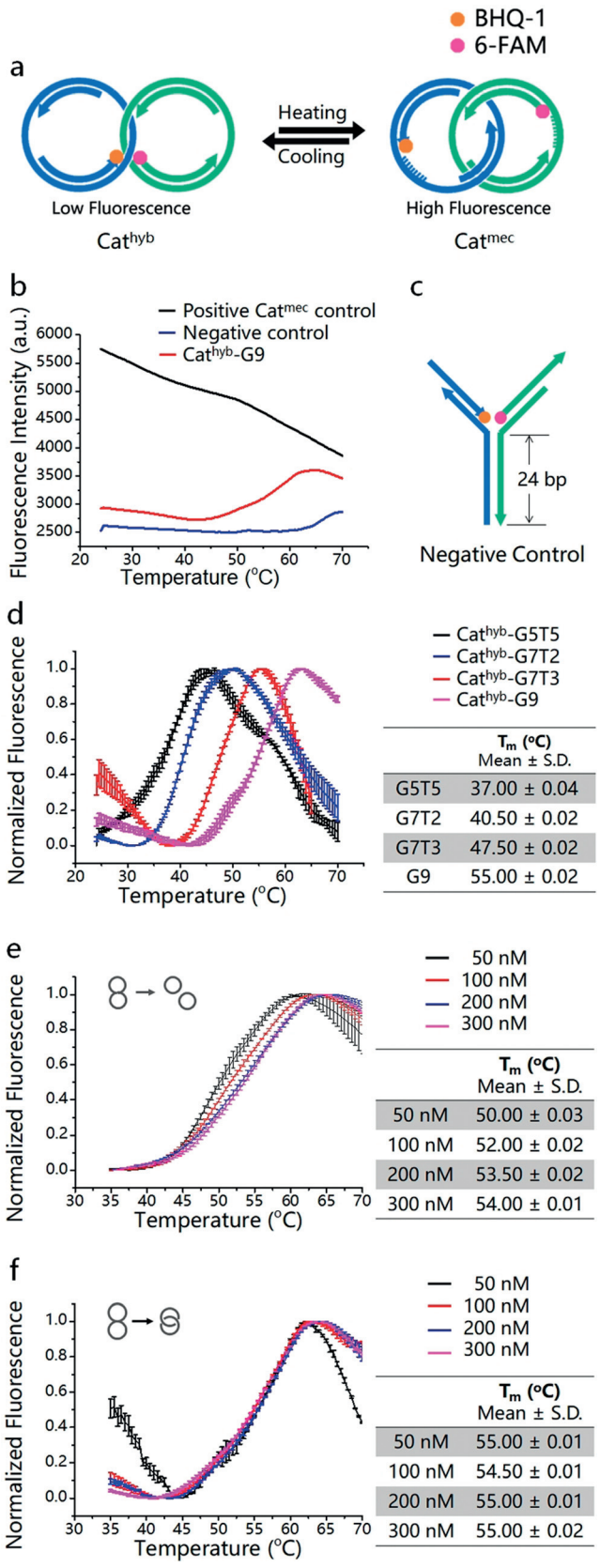

Figure 2. Thermal switching between Cat^{hyb} and Cat^{mec}. a) Schematic depiction of the mechanism of thermal switching of the Cat^{hyb} to Cat^{mec}. b) Temperature-dependent fluorescence intensity of 20 μL of 100 nM Cat^{hyb}-G9 with an initially quenched FAM (red), 20 μL of 100 nM Cat^{mec} positive control that has a non-quenched FAM (black), and 20 μL of 100 nM of the Y-shaped negative control (blue). c) Structure of the Y-shaped negative control construct (for structures and sequences see the Supporting Information, Figure S3 and Table S2). d) Temperature-dependent fluorescence intensity of Cat^{hyb}-G5T5 (black), Cat^{hyb}-G7T2 (blue), Cat^{hyb}-G7T3 (red), and Cat^{hyb}-G9 (pink; S.D., $n=3$). e) Temperature-dependent fluorescence intensity of hybridized but non-interlocked ring A and ring B with HR of G9 at 50 nM (black), 100 nM (red), 200 nM (blue), and 300 nM (pink; S.D., $n=3$). f) Temperature-dependent fluorescence intensity of the Cat^{hyb}-G9 at 50 nM (black), 100 nM (red), 200 nM (blue), and 300 nM (pink; S.D., $n=3$).

The temperature-response range of the Cat^{hyb} is tunable by changing the length and sequence of HR without having to modify the whole nanostructure. As a proof of concept, we synthesized three other Cat^{hyb} ODNs—G5T5, G7T2, and G7T3—with different HR sequences that differ either in length or in their guanine–cytosine (GC) content (Table 1) and measured their melting curves. As shown in Figure 2d, in the DC buffer the melting region of the Cat^{hyb} at 100 nM can change from low temperature (black curve, Cat^{hyb}-G5T5, 24.50 ± 0.01 °C–45.00 ± 0.02 °C, S.D., $n=3$) to high temperature (pink curve, Cat^{hyb}-G9, 42.00 ± 0.01 °C–62.00 ± 0.01 °C, S.D., $n=3$) by increasing the GC content or by increasing the number of base pairs in HR. Additionally, the melting regions of the Cat^{hyb} ODNs are comparable to the T_m of DNA systems that consist of non-interlocked dsDNA strands with the same sequences and the same concentration (Figure S6).

In general, the T_m and melting curves are strongly influenced by strand concentration when two ssDNA strands interact.[12] However, in an interlocked structure, the dsDNA rings will remain interlocked during the conversion of Cat^{hyb} into the Cat^{mec}, which means that the ss-gap on the DNA rings could only hybridize with their counterparts in the same interlocked structure because of the catenation of the rings. This characteristic of DNA catenanes greatly reduces the influence of the strand concentration in the melting process. The T_m and melting region of hybridized but non-interlocked ring A and ring B (Figures 2e,f; sequences are presented in Table S4) with HR of G9 shifted when the concentration of the dsDNA rings increased from 50 nM to 300 nM (Figure 2d); however. the T_m and melting range of the Cat^{hyb}-G9 remained largely unchanged when the concentration of the Cat^{hyb}-G9 increased from 50 nM to 300 nM (Figure 2e). This result indicates that the catenanes are well suited as robust and sensitive nanothermometers since their response to temperature can be finely tuned by changing only the HR and is independent from the concentration of the structure itself.

Subsequently, we studied the thermal reversibility of the conversion of Cat^{hyb} to Cat^{mec}. Since the HR consists of only two short ss-regions, the Cat^{hyb} can be easily restored to its original form at temperatures below T_m. We measured the time-dependent change of fluorescence intensity when the Cat^{mec}-G9 was cooled from 65 °C down to 24 °C, and found that the fluorescence intensity decreased rapidly in the first

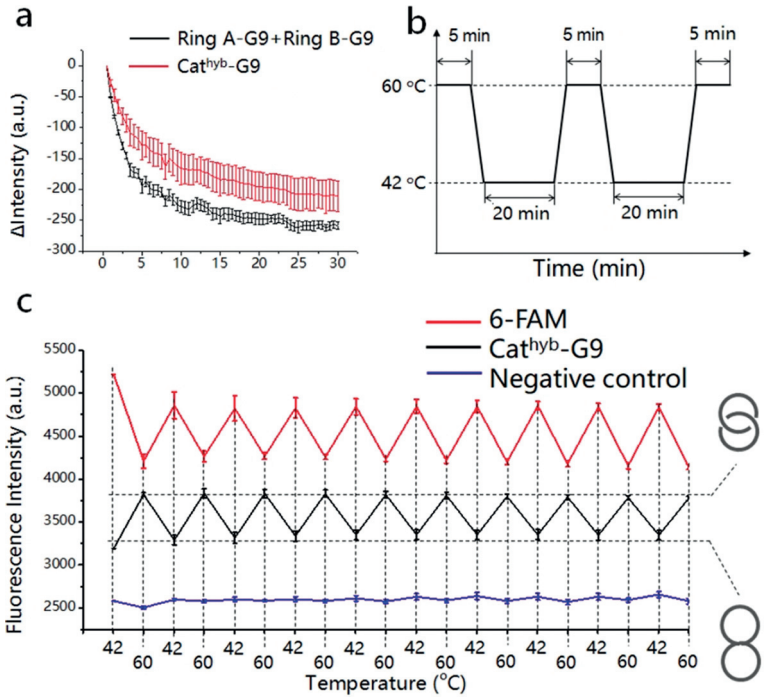

Figure 3. Thermal reversibility of the Cat^{hyb} to Cat^{mec} interconversion. a) Time-dependent change of fluorescence intensity of the mixture of ring A-G9 and ring B-G9 (black, 100 nM) and the Cat^{mec}-G9 (red, 100 nM) in DC buffer (S.D., $n=3$). b) Diagram of the temperature cycling between 42 °C and 60 °C. c) Fluorescence intensity of 6-FAM (red), Cat^{hyb}-G9 (black), and the quenched negative control (blue) at 42 °C and 60 °C (S.D, $n=3$).

20–25 minutes (Figure 3a, red), which was similar to the mixture of ring A-G9 and ring B-G9 (Figure 3a, black). This finding indicates that Cat^{mec} can be converted into Cat^{hyb} without requiring special annealing processes. The thermal reversibility test was performed by a temperature cycling between 42 °C and 60 °C with a fast rate of 3 °C s^{-1}, and the sample was incubated at 42 °C for 20 minutes and at 60 °C for 5 minutes in each cycle (Figure 3b). The fluorescence change of the Cat^{hyb}-G9 showed no indication of fatigue after 10 temperature cycles (Figure 3c; Figure S7). The negative control construct with its longer HR that did not melt at 60 °C remains unchanged during the temperature cycles (Figure 3c, blue). Although each dsDNA ring in the Cat^{hyb}-G9 contains two different ss-regions (Figure 1a), and hybridization to the wrong ss-region would not result in signal quenching, the fluorescence intensity of the Cat^{hyb}-G9 at 42 °C in each temperature cycle remained the same, which indicates that the two dsDNA rings hybridize correctly when the Cat^{mec} is cooled and converts into Cat^{hyb}-G9 because of the specificity of Watson–Crick base pairing.

In conclusion, we have demonstrated design, assembly, characterization by gel electrophoresis, AFM analysis, and fluorescence detection of a new class of thermal responsive nanojoints. The described DNA nanostructures consist of two interlocked dsDNA rings that are connected through a HR and can reversibly switch between the static and mobile state at different temperatures through the melting and rehybridization of its HR. The temperature response range of the nanojoint can be easily fine-tuned by changing the length and/or the GC content of the HR sequence. In comparison with previously reported DNA thermoresponsive systems, these nanojoints provide serval unique features suitable for creating functional temperature-sensitive DNA nanostructures. First, the nanojoint switches from the static state to the mobile state instead of disassembling at high temperature, which provides controlled and confined mobility between different components while keeping the whole nanostructure intact. Second, the nanojoint can be easily reversed without a special annealing process. Finally, unlike systems that consist of separated components, the temperature response range of the interlocked nanojoint remains essentially unaffected by its concentration because of its interlocked structure.

Acknowledgements

This research was supported by the Max-Planck-Society and University of Bonn through a Max-Planck-Fellowship and the Alexander von Humboldt Foundation. Open access funding enabled and organized by Projekt DEAL.

Conflict of interest

The authors declare no conflict of interest.

Keywords: DNA catenanes · DNA nanomachines · DNA nanotechnology · Interlocked DNA nanostructures · Temperature sensors

[1] a) Y. Hu, J. Ren, C.-H. Lu, I. Willner, *Nano Lett.* **2016**, *16*, 4590–4594; b) F. Li, Q. Gao, M. Yang, W. Guo, *Langmuir* **2018**, *34*, 14932–14939; c) T. Li, F. Lohmann, M. Famulok, *Nat. Commun.* **2014**, *5*, 4940; d) T. Patino, A. Porchetta, A. Jannasch, A. Lladó, T. Stumpp, E. Schäffer, F. Ricci, S. Sánchez, *Nano Lett.* **2019**, *19*, 3440–3447; e) C. Wang, Z. Huang, Y. Lin, J. Ren, X. Qu, *Adv. Mater.* **2010**, *22*, 2792–2798; f) S. Modi, C. Nizak, S. Surana, S. Halder, Y. Krishnan, *Nat. Nanotechnol.* **2013**, *8*, 459; g) S. Modi, M. Swetha, D. Goswami, G. D. Gupta, S. Mayor, Y. Krishnan, *Nat. Nanotechnol.* **2009**, *4*, 325–330; h) W. Wang, Y. Yang, E. Cheng, M. Zhao, H. Meng, D. Liu, D. Zhou, *Chem. Commun.* **2009**, *45*, 824–826; i) A. Kuzuya, R. Watanabe, Y. Yamanaka, T. Tamaki, M. Kaino, Y. Ohya, *Sensors* **2014**, *14*, 19329–19335; j) L. N. Green, A. Amodino, H. K. K. Subramanian, F. Ricci, E. Franco, *Nano Lett.* **2017**, *17*, 7283–7288; k) F. Y. Fong, S. S. Oh, C. J. Hawker, H. T. Soh, *Angew. Chem. Int. Ed.* **2016**, *55*, 15258–15262; *Angew. Chem.* **2016**, *128*, 15484–15488.

[2] a) E. S. Andersen, M. Dong, M. M. Nielsen, K. Jahn, R. Subramani, W. Mamdouh, M. M. Golas, B. Sander, H. Stark, C. L. Oliveira, *Nature* **2009**, *459*, 73; b) M. Centola, J. Valero, M. Famulok, *J. Am. Chem. Soc.* **2017**, *139*, 16044–16047; c) R. P. Goodman, M. Heilemann, S. Doose, C. M. Erben, A. N. Kapanidis, A. J. Turberfield, *Nat. Nanotechnol.* **2008**, *3*, 93; d) J. F. Rahbani, A. A. Hariri, G. Cosa, H. F. Sleiman, *ACS Nano*

2015, *9*, 11898 – 11908; e) C. Zhou, Z. Yang, D. Liu, *J. Am. Chem. Soc.* **2012**, *134*, 1416 – 1418; f) A. Amodio, B. Zhao, A. Porchetta, A. Idili, M. Castronovo, C. Fan, F. Ricci, *J. Am. Chem. Soc.* **2014**, *136*, 16469 – 16472; g) D. Y. Zhang, E. Winfree, *J. Am. Chem. Soc.* **2009**, *131*, 17303 – 17314; h) M. Teichmann, E. Kopperger, F. C. Simmel, *ACS Nano* **2014**, *8*, 8487 – 8496.

[3] a) M. W. Haydell, M. Centola, V. Adam, J. N. Valero, M. Famulok, *J. Am. Chem. Soc.* **2018**, *140*, 16868 – 16872; b) X. Liang, H. Nishioka, N. Takenaka, H. Asanuma, *ChemBioChem* **2008**, *9*, 702 – 705; c) F. Lohmann, D. Ackermann, M. Famulok, *J. Am. Chem. Soc.* **2012**, *134*, 11884 – 11887; d) M. Škugor, J. Valero, K. Murayama, M. Centola, H. Asanuma, M. Famulok, *Angew. Chem. Int. Ed.* **2019**, *58*, 6948 – 6951; *Angew. Chem.* **2019**, *131*, 7022 – 7025; e) D. Y. Tam, Z. Dai, M. S. Chan, L. S. Liu, M. C. Cheung, F. Bolze, C. Tin, P. K. Lo, *Angew. Chem. Int. Ed.* **2016**, *55*, 164 – 168; *Angew. Chem.* **2016**, *128*, 172 – 176; f) Y. Yang, M. Endo, K. Hidaka, H. Sugiyama, *J. Am. Chem. Soc.* **2012**, *134*, 20645 – 20653; g) A. T. Veetil, K. Chakraborty, K. Xiao, M. R. Minter, S. S. Sisodia, Y. Krishnan, *Nat. Nanotechnol.* **2017**, *12*, 1183 – 1189; h) P. K. Dutta, R. Varghese, J. Nangreave, S. Lin, H. Yan, Y. Liu, *J. Am. Chem. Soc.* **2011**, *133*, 11985 – 11993; i) M. You, Y. Chen, X. Zhang, H. Liu, R. Wang, K. Wang, K. R. Williams, W. Tan, *Angew. Chem. Int. Ed.* **2012**, *51*, 2457 – 2460; *Angew. Chem.* **2012**, *124*, 2507 – 2510; j) M. Liu, S. Jiang, O. Loza, N. E. Fahmi, P. Šulc, N. Stephanopoulos, *Angew. Chem. Int. Ed.* **2018**, *57*, 9341 – 9345; *Angew. Chem.* **2018**, *130*, 9485 – 9489.

[4] a) J. T. Dias, M. Moros, P. del Pino, S. Rivera, V. Grazú, J. M. de la Fuente, *Angew. Chem. Int. Ed.* **2013**, *52*, 11526 – 11529; *Angew. Chem.* **2013**, *125*, 11740 – 11743; b) O. Franch, F. Iacovelli, M. Falconi, S. Juul, A. Ottaviani, C. Benvenuti, S. Biocca, Y.-P. Ho, B. R. Knudsen, A. Desideri, *Nanoscale* **2016**, *8*, 13333 – 13341; c) D. Gareau, A. Desrosiers, A. Vallée-Bélisle, *Nano Lett.* **2016**, *16*, 3976 – 3981; d) S. Juul, F. Iacovelli, M. Falconi, S. L. Kragh, B. Christensen, R. Frøhlich, O. Franch, E. L. Kristoffersen, M. Stougaard, K. W. Leong, *ACS Nano* **2013**, *7*, 9724 – 9734; e) Y. Xing, E. Cheng, Y. Yang, P. Chen, T. Zhang, Y. Sun, Z. Yang, D. Liu, *Adv. Mater.* **2011**, *23*, 1117 – 1121; f) Z. Yu, N. Li, P. Zheng, W. Pan, B. Tang, *Chem. Commun.* **2014**, *50*, 3494 – 3497; g) J. M. Zuidema, A. Bertucci, J. Kang, M. J. Sailor, F. Ricci, *Nanoscale* **2020**, *12*, 2333 – 2339; h) G. Ke, C. Wang, Y. Ge, N. Zheng, Z. Zhu, C. J. Yang, *J. Am. Chem. Soc.* **2012**, *134*, 18908 – 18911; i) K. Zhang, X. Zhu, F. Jia, E. Auyeung, C. A. Mirkin, *J. Am. Chem. Soc.* **2013**, *135*, 14102 – 14105; j) S. Jeon, J. Turner, S. Granick, *J. Am. Chem. Soc.* **2003**, *125*, 9908 – 9909; k) S. Ebrahimi, Y. Akhlaghi, M. Kompany-Zareh, Å. Rinnan, *ACS Nano* **2014**, *8*, 10372 – 10382.

[5] B. Klinkert, F. Narberhaus, *Cell. Mol. Life Sci.* **2009**, *66*, 2661 – 2676.

[6] a) C.-H. Lu, A. Cecconello, J. Elbaz, A. Credi, I. Willner, *Nano Lett.* **2013**, *13*, 2303 – 2308; b) C.-H. Lu, A. Cecconello, X.-J. Qi, N. Wu, S.-S. Jester, M. Famulok, M. Matthies, T.-L. Schmidt, I. Willner, *Nano Lett.* **2015**, *15*, 7133 – 7137.

[7] a) T. L. Schmidt, A. Heckel, *Nano Lett.* **2011**, *11*, 1739 – 1742; b) J. Valero, N. Pal, S. Dhakal, N. G. Walter, M. Famulok, *Nat. Nanotechnol.* **2018**, *13*, 496.

[8] a) F. Lohmann, J. Valero, M. Famulok, *Chem. Commun.* **2014**, *50*, 6091 – 6093; b) C. H. Lu, X. J. Qi, A. Cecconello, S. S. Jester, M. Famulok, I. Willner, *Angew. Chem. Int. Ed.* **2014**, *53*, 7499 – 7503; *Angew. Chem.* **2014**, *126*, 7629 – 7633.

[9] J. Valero, M. Centola, Y. Ma, M. Škugor, Z. Yu, M. W. Haydell, D. Keppner, M. Famulok, *Nat. Protoc.* **2019**, *14*, 2818 – 2855.

[10] a) D. Ackermann, T. L. Schmidt, J. S. Hannam, C. S. Purohit, A. Heckel, M. Famulok, *Nat. Nanotechnol.* **2010**, *5*, 436 – 442; b) J. Weigandt, C. L. Chung, S. S. Jester, M. Famulok, *Angew. Chem. Int. Ed.* **2016**, *55*, 5512 – 5516; *Angew. Chem.* **2016**, *128*, 5602 – 5606; c) F. Lohmann, J. Weigandt, J. Valero, M. Famulok, *Angew. Chem. Int. Ed.* **2014**, *53*, 10372 – 10376; *Angew. Chem.* **2014**, *126*, 10540 – 10544.

[11] W.-T. Liu, J.-H. Wu, E. S.-Y. Li, E. S. Selamat, *Appl. Environ. Microbiol.* **2005**, *71*, 6453 – 6457.

[12] a) U. Giesen, W. Kleider, C. Berding, A. Geiger, H. Ørum, P. E. Nielsen, *Nucleic Acids Res.* **1998**, *26*, 5004 – 5006; b) R. Owczarzy, P. M. Vallone, F. J. Gallo, T. M. Paner, M. J. Lane, A. S. Benight, *Biopolymers Orig. Res. Biomol.* **1997**, *44*, 217 – 239.

Manuscript received: March 18, 2020
Revised manuscript received: June 12, 2020
Accepted manuscript online: June 22, 2020
Version of record online: July 1, 2020

